Malaysian Journal of Mathematical Sciences 18(2): 445–468 (2024)
https://doi.org/10.47836/mjms.18.2.13

Malaysian Journal of Mathematical Sciences

Journal homepage: https://mjms.upm.edu.my

# MHD Flow of Dusty Jeffrey Fluid Flow Containing Carbon Nano Tubes (CNTs) under Influences of Viscous Dissipation and Newtonian heating

Habib, N. A. N. N.[1], Arifin, N. S.*[2], Zokri, S. M.[3], and Kasim, A. R. M.[4]

[1]*College of Computing, Informatics and Mathematics, Universiti Teknologi MARA (UiTM) Johor Branch, Segamat Campus, 85000 Segamat, Johor, Malaysia*
[2]*College of Computing, Informatics and Mathematics, Universiti Teknologi MARA (UiTM) Johor Branch, Pasir Gudang Campus, 81750 Masai, Johor, Malaysia*
[3]*College of Computing, Informatics and Mathematics, Universiti Teknologi MARA (UiTM) Terengganu Branch, Kuala Terengganu Campus, 21080 Kuala Terengganu, Malaysia*
[4]*Centre for Mathematical Sciences, Universiti Malaysia Pahang Al-Sultan Abdullah, Lebuhraya Persiaran Tun Khalil Yaakob, 26300, Gambang, Pahang, Malaysia*

*E-mail: nursyamilaharifin@uitm.edu.my*
**Corresponding author*

*Received: 9 January 2024*
*Accepted: 20 March 2024*

## Abstract

This current research examines the behaviour of dusty Jeffrey fluid across an inclined stretching sheet with CNTs as well as aligned magnetohydrodynamic (MHD). By utilising the proper similarity transformation variables, the governing partial differential equations (PDEs) of the problem are converted to ordinary differential equations (ODEs). Then, the numerical results are produced by using the Runge-Kutta-Fehlberg (RKF45) approach with the aid of the MAPLE software. The findings include the visual illustrations of the impacts on the velocity and temperature profiles for several pertinent parameters. It clearly shows that the decline in velocity profile of fluid phase was caused by the rise in aligned angle, ratio of relaxation to retardation times, magnetic field and fluid particle interaction parameters. Meanwhile, for every parameter that is involved excluding ratio of retardation time in the fluid, the temperature profile rises in both the fluid and dusty phases. The results of this study add a unique perspective to the existing literature by offering fresh insights on the influence of CNTs and dust particles, examining their impact on two-phase flow over an inclined stretching sheet. This understanding can be utilized in the real-time application where rapid and efficient thermal management is critical such as electronics cooling or energy conversion systems. Furthermore, the inclusion of viscous dissipation and Newtonian heating (NH) effects contributes to the novelty of the research, providing a comprehensive understanding of the complex interactions in this unique fluid flow scenario.

**Keywords:** aligned MHD; Dusty Jeffrey fluid; CNTs; inclined stretching sheet; Newtonian heating.

## Nomenclature

| | |
|---|---|
| $u$ | velocity in $x$-direction $(ms^{-1})$ |
| $v$ | velocity in $y$-direction $(ms^{-1})$ |
| $x$ | horizontal coordinate $(m)$ |
| $y$ | vertical coordinate $(m)$ |
| $u_w$ | velocity of the sheet surface $(ms^{-1})$ |
| $B$ | magnetic field $(T)$ |
| $C$ | specific heat $(J/kg°C)$ |
| $h_s$ | coefficient of heat transfer $(W/m^2/K)$ |
| $g_0$ | gravitational force $(N)$ |
| $T$ | local temperature $(K)$ |
| $T_\infty$ | ambient temperature $(K)$ |
| $T_p$ | temperature of dust particle $(K)$ |
| $Gr_x$ | Grashof number $(-)$ |
| $De$ | Deborah number $(-)$ |
| $M$ | magnetic field parameter $(T)$ |
| $Pr$ | Prandtl number $(-)$ |
| $Ec$ | Eckert number $(-)$ |
| $N$ | mass coefficient of particle phase $(kg/m^3)$ |
| $C_f$ | skin friction coefficient $(N/m^2)$ |
| $Nu_x$ | Nusselt number $(-)$ |
| $q_w$ | surface heat flux $(W/m^2)$ |
| $f(\eta)$ | velocity variable $(-)$ |
| $\theta(\eta)$ | temperature variable $(-)$ |
| $Re_x$ | Reynold number $(-)$ |

## Greek symbols

| | |
|---|---|
| $\mu$ | dynamic viscosity $(kg/ms)$ |
| $\rho$ | density $(kg/m^3)$ |
| $\sigma$ | electrical conductivity $(S/m)$ |
| $\alpha$ | aligned angle $(°)$ |
| $\alpha_0$ | angle of inclined stretching sheet $(°)$ |
| $\beta_T$ | thermal expansion coefficient $(K^{-1})$ |
| $\kappa$ | thermal conductivity $(W/mk)$ |
| $\tau_v$ | velocity relaxation time of particle $(s)$ |
| $\tau_T$ | thermal relaxation time of particle $(s)$ |
| $\kappa_w$ | rate of heat transfer $(W)$ |
| $\lambda$ | ratio of relaxation to retardation times$(-)$ |
| $\lambda_1$ | retardation times $(s)$ |
| $\nu$ | kinematic viscosity $(m^2/s)$ |
| $\eta$ | similarity variable $(-)$ |
| $\gamma$ | conjugate parameter of NH $(-)$ |
| $\beta$ | fluid particle interaction parameter $(-)$ |
| $\phi$ | volume fraction parameter $(-)$ |

## Subscript

| | |
|---|---|
| $f$ | fluid |
| $nf$ | nanofluid |
| $p$ | dust particles |

## 1 Introduction

In numerous areas of industrial and manufacturing operations, the practical use of heat transfer has become necessary. Many studies have focused on the significance of heat transmission and flow across stretching surfaces in various geometries due to its many applications in science and industry, including the extrusion of metal and polymer sheets, the stretching of plastic films, the cooling of metallic or glass plates, the aerodynamic shaping of plastic sheets, the manufacturing of artificial fibres and wire drawing [11]. The dynamics of two-phase flow involving non-Newtonian fluids have additionally drawn a lot of attention because of their importance in many fields including dust collection, powder technology, atmospheric fallout and nuclear reactor cooling. Izani and Ali [19] explored how a magnetic field affected the convective heat transfer and boundary layer flow of dusty Jeffrey fluid across an exponentially stretching surface. Another study on the two-phase MHD fluid flow of continuous dusty particles and non-Newtonian Darcy fluids between parallel plates was studied by Attia et al. [8]. Later, Izani and Ali [20] continued their investigation of the dusty Jeffrey fluid flow in a transverse magnetic field across the same surface. Kasim et al. [31] analysed convective transport involving the interaction between fluid and solid focusing on how dust particles influence the behaviour of Casson fluid.

Jeffrey fluid is a type of non-Newtonian fluid that exhibits both elastic and viscous characteristics which makes it suitable for modelling materials that show both solid-like and liquid-like behaviour. The shear-thinning property of Jeffrey fluids, where viscosity decreases with increased shear rate, is particularly useful to describe the flow of various complex substances like polymer

melts or certain biological fluids. Understanding Jeffrey fluid characteristics helps to provide insights into how it responds to forces and deformations, which is crucial for fields like materials science, biofluid dynamics, and industrial processes. Due to this, numerous researchers initiate their investigations on Jeffrey fluid with the aim to explore its diverse practical uses. Ahmad et al. [1] discussed the steady two-dimensional MHD boundary layer flow and heat transfer of a Jeffrey fluid over a stretched sheet in the presence of viscous dissipation. Later, Tlili [39] explored the mixed convective boundary layer flow over an inclined stretching sheet in Jeffrey fluid with the presence of heat source/sink and viscous dissipation effect. Focusing on MHD heat transfer flow, Kumar [27] investigated the differential transform technique for transient and incompressible Jeffrey fluid flow from a stretching sheet. Another study on the unsteady boundary layer flow with heat and mass transfer of Jeffrey fluid has been carried out by Nabwey et al. [32]. Recently, Anusha et al. [7] studied on the MHD flow and heat transfer of Jeffrey fluid due to a stretching/shrinking surface embedded with CNTs considering the effects of thermal radiation, heat source/sink parameters and Navier's slip.

The MHD flow is the physical studies on the influence of magnetic fields on the dynamic conducting fluid. It has many important applications in science and technology, mainly engineering. For instance, the cooling of reactors, the petroleum industry, metrology, power generators and heat exchangers. Keeping interest in the MHD's various uses, many scholars begin their research by considering the MHD flow in their studies [14, 29, 41]. Ahmed et al. [3] performed research on the exact solution for MHD Jeffrey fluid convective heat transfer across a stretching sheet. By considering stretching vertical surface in a porous medium, Ahmad et al. [2] addressed the flow and heat transfer of MHD Jeffrey fluid in a mixed convection boundary layer. Meanwhile, Reddy et al. [34] examined the MHD Jeffrey fluid over a stretching vertical surface with an accelerated porous plate with a heat source. Recently, Habib et al. [13] documented a study on the motion of Jeffrey fluid across an exponentially stretching sheet with viscous dissipation effects that included aligned MHD embedded with CNTs. Another study on the effect of pressure gradient in MHD flow of a tri-hybrid Newtonian nanofluid in a circular channel has been carried out by Shahzad et al. [37].

The development of advanced fluids has led to the invention of nanofluid, one of the non-Newtonian fluid models that enhances the fluid's thermal conductivity and helps the equipment to transfer heat. The pioneers of nanofluid, Choi and Eastman [9] discovered that adding nanoparticles to a conventional base fluid exhibits high thermal conductivities and improves heat transfer. The presence of nanoparticles in dusty fluid can influence its rheological properties, including viscosity and thermal conductivity. Nanoparticles typically have a large surface area to volume ratio which can lead to enhanced interactions with the surrounding fluid molecules and results in the increasing of viscosity. Moreover, nanoparticles can affect the thermal conductivity of dusty fluid which can impact the temperature distribution within the fluid by altering the thermal expansion behaviour of the dust particles and their interaction with the surrounding fluid. As a results, many researchers embark on investigation into nanoparticles to discover its wide range of practical applications. Khan [23] used blood as base fluid and single-wall carbon nanotubes are suspended in blood as nanoparticles to explore a new idea of Atangana and Baleanu fractional derivatives in human blood flow. Later, Khan et al. [25] discussed the importance of fractal fractional derivative with a power-law kernel for heat transfer in a drilling nanofluid with clay nanoparticle in a vertical channel. Another study on the nanofluids has been carried out by Khan [24] by examining the impact of convective heat transfer through an inclined plate by utilizing the CNTs.

Among all nanoparticles, CNTs stand out among various nanoparticles due to their excellent mechanical, electrical and thermal conductivities, making them highly suitable for a broad variety of functions. To date, many researchers have attempted to consider the CNTs in their studies on boundary layer flow. Anuar et al. [5] consider the moving plate with a slip effect to deter-

mine the motion and heat transmission properties of CNTs in single-wall and multi-wall which are employed with kerosene and water as basic fluids. Another study on the effect of MHD on the 2D mixed convection fluid flow past a nonlinearly deforming vertical surface in CNTs has been reported by Anuar et al. [6]. By taking the stability analysis into account, Anuar et al. [4] evaluated the influence of a transverse magnetic field with CNTs on the stagnation point flow along a nonlinear stretching or shrinking sheet. Recently, Ishak et al. [18] investigated the flow of CNTs under the influence of aligned MHD across a static or moving wedge by considering the convective boundary conditions.

NH is one of the heating conditions that has been commonly employed in the study of convection boundary layer flow over different surfaces. It refers to a heat transfer phenomenon where temperature of a fluid increases linearly with distance from a heated surface. This heating mechanism assumes that the temperature increase within the fluid is directly linked to the local heat flux at the boundary surface. NH provides a realistic representation of heat transfer model generally in a system where heat is transferred from a surface to a flowing fluid. Merkin [30] was the first to investigate the different types of temperature distributions at the wall in which NH was one of them. Focusing on the NH condition, Hussanan et al. [22] explored the impact of MHD flow of a Casson fluid and heat transfer to a nonlinear stretching sheet. Meanwhile, Kassim et al. [35] investigated the interaction between solid and fluid under combined convective Jeffrey flow and radiation effect over a vertical stretching sheet. In the MHD flow of Jeffrey fluid, Redwan et al. [17] emphasized the numerical analysis of boundary layer flow and heat transfer over a moving flat plate with NH. On the other hand, Rehman et al. [36] carried out a numerical analysis on the heated non-Newtonian fluid with NH effect towards two different stretched surfaces which are plate and cylinder.

In all of the above-mentioned investigations, it has been observed that most of the research has treated two-phase flow and nanoparticles separately. None of them was identified to deliberate the involvement of the CNTs in the fluid and dust phases. Hence, contemplating the impacts of NH and viscous dissipation, the current study examines the analysis of the aligned MHD dusty Jeffrey fluid with CNTs across an inclined stretching sheet. The three main objectives of the research are to develop mathematical models for Jeffrey fluid and dusty Jeffrey fluid with CNT particles over an inclined stretching sheet, to solve the models using the RKF45 method with the help of MAPLE software, and to analyse the influence of several pertinent parameters on the velocity and temperature profiles, as well as the skin friction coefficient and Nusselt number.

## 2 Problem Formulation

The streamline and incompressible 2D flow involving the dusty Jeffrey fluid across an inclined stretching sheet is investigated. This interaction occurs by looking into the impacts of viscous dissipation and NH on the motion of an aligned magnetic field. The methodology presented by Tiwari and Das is utilised to solve the proposed mathematical problem [38]. Assume that the coordinate system is configured so that the $x$-axis aligns with the inclined stretching surface and the $y$-axis is at the right angle to the sheet where the bottom of the sheet is heated by NH. The velocity of the inclined stretching sheet is represented by $u_w(x) = ax$ where $a$ and $x$ are the positive constant and the uniform magnetic field of strength, $\beta$ flows with an aligned angle, $\alpha$ in the range of $0^\circ$ to $90^\circ$ as in Figure 1.

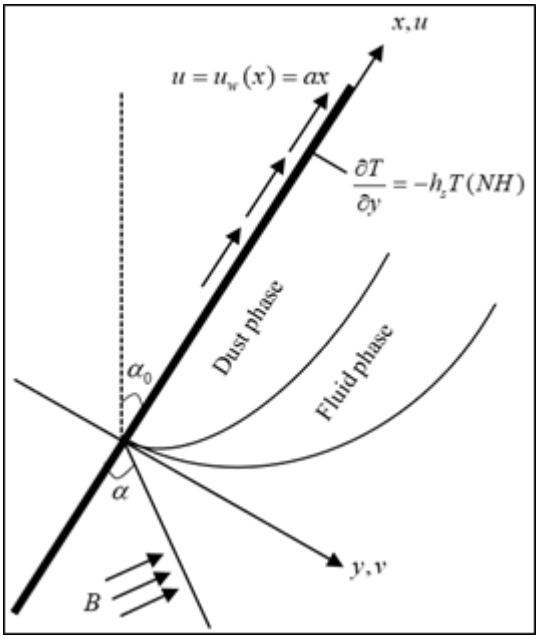


Figure 1: The flow configuration of Dusty Jeffrey fluid.

The state equations for Jeffrey fluid can be denoted as;

$$\frac{\partial u}{\partial x} + \frac{\partial v}{\partial y} = 0, \tag{1}$$

$$\begin{aligned} u\frac{\partial u}{\partial x} + v\frac{\partial v}{\partial y} = {} & \frac{\mu_{nf}}{\rho_{nf}(1+\lambda)}\left[\frac{\partial^2 u}{\partial y^2} + \lambda_1\left(u\frac{\partial^3 u}{\partial x \partial y^2} + v\frac{\partial^3 u}{\partial y^3} - \frac{\partial u}{\partial x}\frac{\partial^2 u}{\partial y^2} + \frac{\partial u}{\partial y}\frac{\partial^2 u}{\partial x \partial y}\right)\right] \\ & - \frac{\sigma_{nf}}{\rho_{nf}}B^2 u \sin^2\alpha + g_0\left[(\beta_T)_{nf}(T - T_\infty)\right]\cos\alpha_0 + \frac{\rho_p}{\rho_{nf}\tau_v}(u_p - u), \end{aligned} \tag{2}$$

$$\begin{aligned} u\frac{\partial T}{\partial x} + v\frac{\partial T}{\partial y} = {} & \frac{\kappa_{nf}}{(\rho C_p)_{nf}}\frac{\partial^2 T}{\partial y^2} + \frac{\mu_{nf}}{(\rho C_p)_{nf}(1+\lambda)}\left[\left(\frac{\partial u}{\partial y}\right)^2 + \lambda_1\left(u\frac{\partial u}{\partial y}\frac{\partial^2 u}{\partial x \partial y} + v\frac{\partial u}{\partial y}\frac{\partial^2 u}{\partial y^2}\right)\right] \\ & + \frac{\rho_p C_s}{\tau_T(\rho C_p)_{nf}}(T_p - T), \end{aligned} \tag{3}$$

where Equations (1)–(3) indicates the continuity, momentum and energy equations. Meanwhile, the state equations for dust particles are listed below;

$$\frac{\partial u_p}{\partial x} + \frac{\partial v_p}{\partial y} = 0, \tag{4}$$

$$u_p\frac{\partial u_p}{\partial x} + v_p\frac{\partial v_p}{\partial y} = -\frac{1}{\tau_v}(u_p - u), \tag{5}$$

$$u_p\frac{\partial T_p}{\partial x} + v_p\frac{\partial T_p}{\partial y} = -\frac{1}{\tau_T}(T_p - T), \tag{6}$$

where the velocity elements along $x$-axis are $u$ and $u_p$, meanwhile, for $y$-axis are $v$ and $v_p$. $\lambda$, $\lambda_1$, $g_0$, $\mu_{nf}$, $\rho_{nf}$, $\sigma_{nf}$, $\kappa_{nf}$, $(C_p)_{nf}$ and $(\beta_T)_{nf}$ denote the ratio of relaxation to retardation times, retardation times, gravitational force, angle of inclined stretching sheet, dynamic viscosity, density, electrical conductivity, thermal conductivity, specific heat at constant pressure and thermal

expansion coefficient for nanofluid phase. Then, $C_s, \tau_v$ and $\tau_T$ indicate the specific heat, velocity relaxation time and thermal relaxation time of dust phase. The thermophysical properties of nanofluid and CNTs are displayed in Table 1 and 2.

Table 1: Thermophysical properties of nanofluid.

| **Properties** | **Nanofluid** |
|---|---|
| Density | $\rho_{nf} = (1-\phi)\rho_f + \phi\rho_{CNT}$ |
| Heat capacity | $(\rho C_p)_{nf} = (1-\phi)(\rho C_p)_f + \phi(\rho C_p)_{CNT}$ |
| Dynamic viscosity | $\mu_{nf} = \dfrac{\mu_f}{(1-\phi)^{2.5}}$ |
| Thermal diffusivity | $\alpha_{nf} = \dfrac{\kappa_f}{(\rho C_p)_{nf}}$ |
| Thermal conductivity | $\dfrac{\kappa_{nf}}{\kappa_f} = \dfrac{(1-\phi) + 2\phi\left(\dfrac{\kappa_{CNT}}{\kappa_{CNT}-\kappa_f}\right)\ln\left(\dfrac{\kappa_{CNT}-\kappa_f}{2\kappa}\right)}{(1-\phi) + 2\phi\left(\dfrac{\kappa_{CNT}}{\kappa_{CNT}-\kappa_f}\right)\ln\left(\dfrac{\kappa_{CNT}+\kappa_f}{2\kappa}\right)}$ |
| Electrical conductivity | $\dfrac{\sigma_{nf}}{\sigma_f} = 1 + \dfrac{3\left(\dfrac{\sigma_{CNT}}{\sigma_f} - 1\right)\phi}{\left(\dfrac{\sigma_{CNT}}{\sigma_f} + 2\right) - 3\left(\dfrac{\sigma_{CNT}}{\sigma_f} - 1\right)\phi}$ |

Table 2: Thermophysical properties of CNTs [26].

| **Properties** | **Base Fluids** | **Nanoparticle** |
|---|---|---|
| | **Water** ($Pr = 7$) | **Single-Wall CNTs** |
| $\rho(kg/m^3)$ | 1053 | 2600 |
| $C_p(J/kgK)$ | 3594 | 425 |
| $k(W/mK)$ | 0.492 | 6600 |

Equations (1)–(6) are subjected to the following boundary conditions;

$$\begin{gathered} u = u_w(x) = ax, \quad v = 0, \quad \frac{\partial T}{\partial y} = -h_s T \quad \text{at} \quad y = 0, \\ u \to 0, \quad v \to 0, \quad T \to T_\infty, \quad u_p \to 0, \quad v_p \to v, \quad T_p \to T_\infty \quad \text{as} \quad y \to \infty, \end{gathered} \tag{7}$$

where $h_s, T, T_\infty$ and $T_p$ are the coefficient of heat transfer, local temperature, ambient temperature and temperature of dust particles, respectively. In solving the problem formulation, it is necessary to utilise the following similarity transformation. To facilitate this, the stream function, $\psi$ is defined as $u = \partial\psi/\partial y$ and $u = -\partial\psi/\partial x$ . Thus, the similarity transformations can be expressed as [21];

$$\begin{gathered} \eta = \left(\frac{a}{v}\right)^{\frac{1}{2}} y, \quad u = axf'(\eta), \quad v = -(av)^{\frac{1}{2}} f(\eta), \quad \theta(\eta) = \frac{T - T_\infty}{T_\infty}, \\ u_p = axF'(\eta), \quad v_p = -(av)^{\frac{1}{2}} F(\eta), \quad \theta_p(\eta) = \frac{T_p - T_\infty}{T_\infty}, \end{gathered} \tag{8}$$

where $\eta$ is the similarity variable, $f(\eta)$ signifies the velocity of fluid, $F(\eta)$ is the velocity of dust phase, $\theta(\eta)$ represents the dimensionless fluid temperature and $\theta_p(\eta)$ is the temperature of dust phase. By utilising Equation (8), Equations (1)–(6) become;

$$\frac{\mu_{nf}/\mu_f}{\rho_{nf}/\rho_f}\Big[f''' + De(f''^2 - ff^{iv})\Big] + (1+\lambda)(ff'' - f'^2) \\ -\frac{\sigma_{nf}/\sigma_f}{\rho_{nf}/\rho_f}(1+\lambda)Mf'\sin^2\alpha + (1+\lambda)d\theta\cos\alpha_0 + (1+\lambda)\beta N(F'-f') = 0, \tag{9}$$

$$\frac{1}{Pr}\frac{\kappa_{nf}/\kappa_f}{(\rho C_p)_{nf}/(\rho C_p)_f}\theta'' + f\theta' + \frac{\mu_{nf}/\mu_f}{(C_p)_{nf}(1+\lambda)/(\rho C_p)_f}Ec\Big[f''^2 + De(f'f''^2 - ff''f''')\Big] \\ +c\beta N(\theta_p - \theta) = 0, \tag{10}$$

$$F'^2 - FF'' + \beta[F' - f'] = 0, \tag{11}$$

$$\theta_p' F - \frac{2\beta}{3bPr}(\theta_p - \theta) = 0, \tag{12}$$

and the transformed boundary conditions can be expressed as follows;

$$f(0) = 0, \quad f'(0) = 1, \quad \theta'(0) = -\gamma(1+\theta(0)) \quad \text{at} \quad \eta = 0, \\ f'(\eta) \to 0, \quad f''(\eta) \to 0, \quad F(\eta) \to f(\eta), \quad F'(\eta) \to 0, \quad \theta(\eta) \to (0), \quad \theta_p(\eta) \to 0 \quad \text{as} \quad \eta = 0, \tag{13}$$

where $\gamma$ is the conjugate parameter of NH. The geometry of the inclined stretching sheet is subjected to the thermal boundary condition of NH where as the heat transfer rate increase, the wall temperature increase and vice versa. Next, the involved parameters can be expressed as;

$$De = \lambda_1 a, \qquad M = \frac{\sigma_f B^2}{\rho_f a}, \qquad Pr = \frac{(\mu C_p)_f}{\kappa_f}, \qquad Ec = \frac{u_w^2}{(C_p)_f T_\infty}, \\ Gr_x = \frac{g_0 T_\infty (\beta_T)_{nf}}{a^2 x}, \qquad b = \frac{C_s}{C_p}, \qquad N = \frac{\rho_p}{\rho_{nf}}, \qquad \beta = \frac{1}{\tau_v a}, \qquad \gamma = h_s\Big(\frac{\nu}{a}\Big)^{\frac{1}{2}}, \tag{14}$$

which represent the Deborah number, magnetic field parameter, Prandtl number, Eckert number [12, 15], Grashof number, specific heat ratio of mixture, mass concentration of particle phase and fluid particle interaction parameter, respectively. $\rho_f$, $\mu_f$, $(C_p)_f$, $\kappa_f$, $\rho_p$ and $\nu$ are for the density, dynamic viscosity, specific heat at constant pressure, thermal conductivity of fluid phase, density of dust particle and kinematic viscosity. Furthermore, Equations (9)–(12) must conform to the similarity transformation outlined in Equation (8), where the solutions exclusively rely on the variable $\eta$ . To achieve this, it is necessary to eliminate variable $x$ so that the Grashof number in Equation (9) is treated as constant. Consequently, $Gr_x$ is redefined by assuming,

$$(\beta_T)_{nf} = cx, \tag{15}$$

where $c$ is constant. Thus, the Grashof number can be written as [28],

$$Gr = \frac{g_0 T_\infty c x}{a^2 x} = \frac{g_0 T_\infty c}{a^2}. \tag{16}$$

Moreover, this paper studied the physical quantities of the shear stress rate and heat transfer rate which are denoted by the skin friction coefficient, $C_f$ and the Nusselt number, $Nu_x$ with the expressions,

$$C_f = \frac{\tau_w}{\rho_f u_w^2}, \qquad Nu_x = \frac{x q_w}{\kappa_f (T - T_\infty)}, \tag{17}$$

in which,

$$\tau_w = \left(\frac{\mu_{nf}}{1+\lambda}\right)\left[\frac{\partial u}{\partial y} + \lambda_1\left(u\frac{\partial^2 u}{\partial x \partial y} + v\frac{\partial^2 u}{\partial y^2}\right)\right], \qquad q_w = -\kappa_{nf}\left(\frac{\partial T}{\partial y}\right)_{y=0}, \tag{18}$$

where $\tau_w$ and $q_w$ are the rate of heat transfer and the surface heat flux, respectively. By using the similarity transformation variable stated in Equation (8), Equations (17) and (18) becomes;

$$\begin{aligned}(Re_x)^{\frac{1}{2}} C_f &= \frac{\mu_{nf}}{\mu_f(1+\lambda)}\Big[f'' + De(f'f'' - f''')\Big],\\ (Re_x)^{\frac{1}{2}} Nu_x X^{-1} &= \gamma\frac{\kappa_{nf}}{\kappa_f}\left(\frac{1}{\theta(\eta)+1}\right),\end{aligned} \tag{19}$$

where $Re_x = \dfrac{a}{\upsilon_f}$ is the Reynolds number and $X^{-1} = \sqrt{x}$.

## 3 Numerical Procedure

To obtain the numerical solutions for the given problem, the RKF45 method is employed. By applying similarity transformation variables as indicated in Equation (8), the governing Equations (1)–(6) are first converted into ODEs (9)–(12). Subsequently, Equations (9)–(12) are interpreted into computer programming languages and solved by applying the RKF45 approach. The RKF45 method is advantageous for solving ordinary differential equations due to its adaptive step size capability, allowing it to efficiently handle regions of rapidly changing solutions while maintaining accuracy. The method is also applicable to a wide range of differential equation problems encountered in scientific and engineering contexts. Next, the built-in MAPLE function named dsolve command is used to programme the proposed problem. The effectiveness of this method depends on choosing the appropriate step size, $h$ during the computation to achieve a reliable estimation of the expected error, $R$ . At every step, the process involves computing and comparing two different approximations. If $R$ exceeds the error tolerance, $\varepsilon$ , the step size is decreased and the current step is recalculated. Conversely, if $R$ is less than $\varepsilon$ , the current step is maintained and $h$ is increased for the next step. The formula for the RKF45 method, along with its numerical algorithm can be described as the following [40, 33];

$$\begin{aligned}
k_1 &= hf(x_1, y_1),\\
k_2 &= hf\left(x_i + \frac{1}{4}h, y_i + \frac{1}{4}k_1\right),\\
k_3 &= hf\left(x_i + \frac{3}{8}h, y_i + \frac{3}{32}k_1 + \frac{9}{32}k_2\right),\\
k_4 &= hf\left(x_i + \frac{12}{13}h, y_i + \frac{1932}{2197}k_1 - \frac{7200}{2197}k_2 + \frac{7296}{2197}k_3\right),\\
k_5 &= hf\left(x_i + h, y_i + \frac{439}{216}k_1 - 8k_2 + \frac{3680}{513}k_3 - \frac{845}{4104}k_4\right),\\
k_6 &= hf\left(x_i + \frac{1}{2}h, y_i - \frac{8}{27}k_1 + 2k_2 - \frac{3544}{2565}k_3 + \frac{1859}{4104}k_4 - \frac{11}{40}k_5\right).
\end{aligned}$$

The approximation of the fourth and fifth orders to the previous six steps are

$$\begin{aligned}
y_{i+1} &= y_i + \frac{25}{216}k_1 + \frac{1408}{2565}k_3 + \frac{2197}{4101}k_4 - \frac{1}{5}k_5,\\
z_{i+1} &= y_i + \frac{16}{135}k_1 + \frac{6656}{12825}k_3 + \frac{28561}{56430}k_4 - \frac{9}{50}k_5 + \frac{2}{55}k_6 40k_5,
\end{aligned}$$

with optimal step size, $\delta = 0.84\left(\frac{\varepsilon}{R}\right)^{\frac{1}{4}}$ - where $R = \frac{1}{h}|z_{i+1} - y_{i+1}|$. Next, the generated results must be compared with the previous published studies for validation purpose.

## 4 Results and Discussions

In this section, numerical results from the obtained mathematical model are displayed graphically by adjusting the values of the involved parameters which are $\lambda, M, \alpha, \beta$, volume fraction $(\phi)$ and conjugate parameter of NH $(\gamma)$ on the velocity and temperature profiles of fluid and dust phases. Incorporating both fluid and dust phases in the graphs is essential to understand the behaviour of the system. The interaction between fluid and dust phases can reveal the way both phases influence and affect each other. Furthermore, each parameter will be individually examined in the graphical results and the parameter value will be selected based on the asymptotic behaviour observed in the graphs. The displayed results are computed by setting the fixed value for certain parameters such as $Pr = 7$, $De = N = 0.2$, $Ec = \gamma = 0.3$, $b = 0.01$, $M = 0.5$ and $c = d = \lambda = \phi = \beta = 0.1$. Table 3 presents the comparison between the current solution and previous findings reported by Hayat et al. [16], who conducted an analytical study on Jeffrey fluid and the numerical results obtained by Dalir et al. [10], for $f''(0)$. The results indicate a strong agreement between the outcomes of this study and the previously published research.

Table 3: Comparison of $f''(0)$ for various values of $De$ when $\phi = M = d = \beta = 0$.

| $De$ | **Hayat et al. [17]** | **Dalir et al. [36]** | **Present,** $f''(0)$ |
|---|---|---|---|
| 0.001 | $-1.09544512$ | $-1.09641580$ | $-1.0954031$ |
| 0.200 | $-1.00000000$ | $-1.00124052$ | $-1.0000317$ |
| 0.400 | $-0.92582010$ | $-0.92724220$ | $-0.9258127$ |
| 0.600 | $-0.86602540$ | $-0.86755715$ | $-0.8660372$ |

Meanwhile, Table 4 displays the data on the $-C_f Re_x^{\frac{1}{2}}$ and $Nu_x Re_x^{\frac{-1}{2}} X^{-1}$ for various parameters. The data reveals a notable decrease in the values of $-C_f Re_x^{\frac{1}{2}}$ as parameters $\lambda$ and $\gamma$ increases, which indicate a smoother flow of fluids along the sheet. The opposite trend is observed for $\beta$, $\phi$ and $De$ since the increase in parameter values leads to more interactions between the fluid and particles at the surface, where additional resistance and friction will be created. Additionally, it can be noticed that the increasing values of $\lambda$ and $\gamma$ lead to the increasing values of $Nu_x Re_x^{\frac{-1}{2}} X^{-1}$ over the remaining parameters. Hence, the heat efficiency has increased since the increase in the value of parameters has enhanced the convective heat transfer in the fluid flow. Thus, it can be suggested that the numerical results for the parameters involved in this problem can be considered as a useful reference for future research.

Table 4: Variation of $-C_f Re_x^{\frac{1}{2}}$ and $Nu_x Re_x^{\frac{-1}{2}} X^{-1}$ for various values of $\beta$, $\lambda$, $\phi$, $De$ and $\gamma$.

| $\beta$ | $\lambda$ | $\phi$ | $De$ | $\gamma$ | $-C_f Re_x^{\frac{1}{2}}$ | $Nu_x Re_x^{\frac{-1}{2}} X^{-1}$ |
|---|---|---|---|---|---|---|
| 1.0 | 0.1 | 0.01 | 0.2 | 0.3 | 1.371928880 | 9892.178991 |
| 1.5 | 0.1 | 0.01 | 0.2 | 0.3 | 1.384728174 | 9836.960192 |
| 2.0 | 0.1 | 0.01 | 0.2 | 0.3 | 1.393219618 | 9800.716936 |
| 0.5 | 0.2 | 0.01 | 0.2 | 0.3 | 1.758931634 | 7509.059770 |
| 0.5 | 0.3 | 0.01 | 0.2 | 0.3 | 1.702931037 | 7558.828975 |
| 0.5 | 0.4 | 0.01 | 0.2 | 0.3 | 1.653067634 | 7604.760257 |
| 0.5 | 0.1 | 0.02 | 0.2 | 0.3 | 1.306755449 | 10184.73784 |
| 0.5 | 0.1 | 0.03 | 0.2 | 0.3 | 1.332561816 | 10073.91101 |
| 0.5 | 0.1 | 0.04 | 0.2 | 0.3 | 1.358942628 | 9964.495556 |
| 0.5 | 0.1 | 0.01 | 0.4 | 0.3 | 1.496943861 | 10147.19231 |
| 0.5 | 0.1 | 0.01 | 0.6 | 0.3 | 1.673498326 | 10016.42373 |
| 0.5 | 0.1 | 0.01 | 0.8 | 0.3 | 1.823190648 | 9900.646944 |
| 0.5 | 0.1 | 0.01 | 0.2 | 0.4 | 1.316204842 | 12319.56129 |
| 0.5 | 0.1 | 0.01 | 0.2 | 0.5 | 1.313353387 | 14171.44217 |
| 0.5 | 0.1 | 0.01 | 0.2 | 0.6 | 1.310075229 | 15750.37357 |

The velocity and temperature profiles for different values of $\lambda$ are displayed in Figures 2 and 3. In Figure 2, it is evident that the velocity declines as $\lambda$ increases in both fluid and dust phases. This phenomenon occurs due to the increases in resistance caused by higher $\lambda$ . As $\lambda$ rises, there will be a greater constraint on the movement of fluid and dust particles which results in the depletion in velocities. Furthermore, the elevated in $\lambda$ also implies in higher viscosity which causes the deceleration of velocity profiles since the fluid requires more time to align its velocity with the equilibrium state. Meanwhile, Figure 3 shows the temperature profile decreases with an increase in $\lambda$ for fluid phase but behaves oppositely in the dust phase. The increasing of $\lambda$ has resulted in the reduction of the thermal activity and hindered the heat transfer in fluid phase which caused the decreasing in temperature profiles due to the greater resistance to thermal flow.

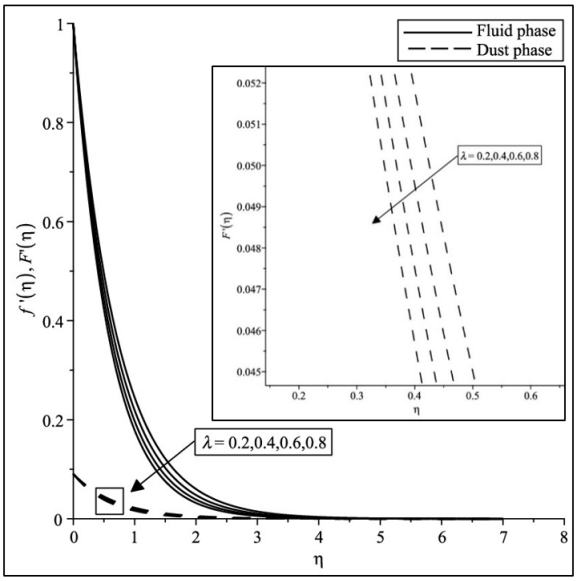


Figure 2: Velocity profiles for various values of $\lambda$.

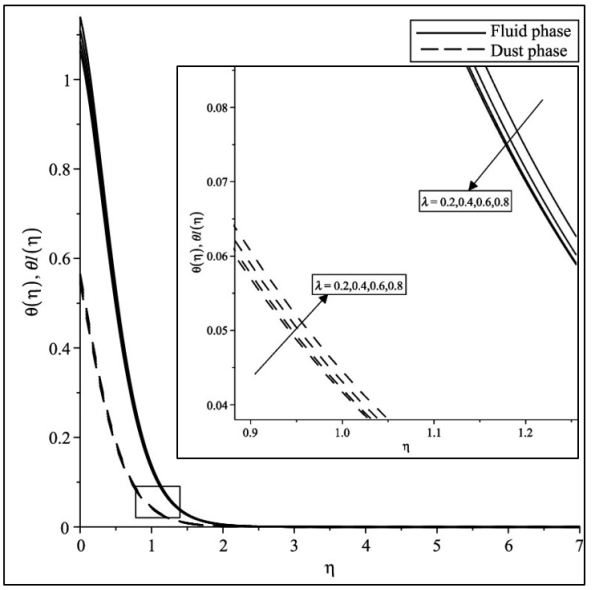


Figure 3: Temperature profiles for various values of $\lambda$.

Next, Figures 4 to 7 display the variation of velocity and temperature profiles of the fluid and dust phases vary with $M$ and $\alpha$ . The figures provide clear evidence that both parameters exhibit a similar tendency towards the velocity and temperature profiles for all phases. Figures 4 and 6 demonstrate a reduction in velocity profile as the parameters and are increased. This outcome can be attributed to the resistance of the fluid movement caused by the Lorentz force, which subsequently decelerates the motion of fluid and dust particles. This finding thereby indicates that an increment of $M$ and $\alpha$ slows down the fluid motion. Furthermore, it is noteworthy that the temperature profile rises when $M$ and $\alpha$ improves for both phases, as shown in Figures 5 and 7.

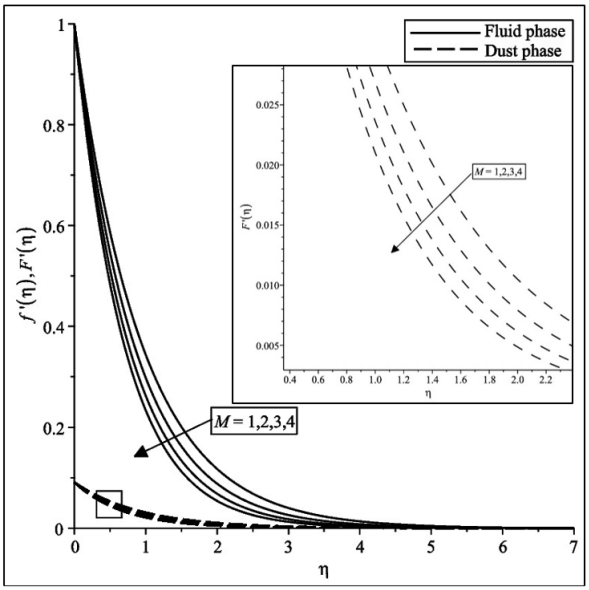


Figure 4: Velocity profiles for various values of $M$.

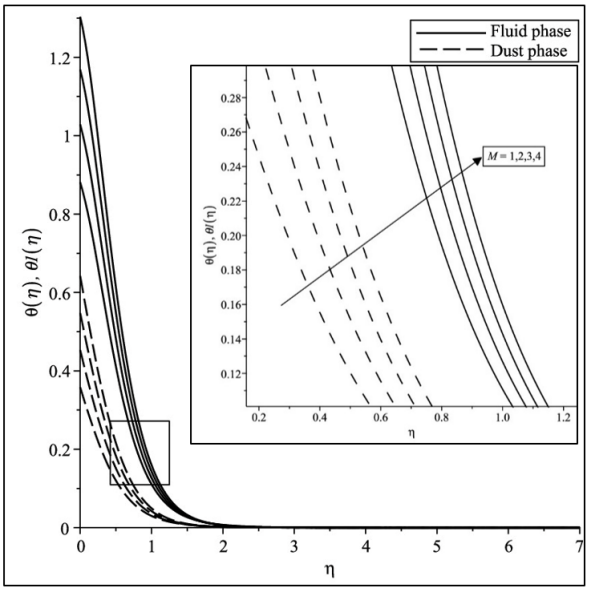


Figure 5: Temperature profiles for various values of $M$.

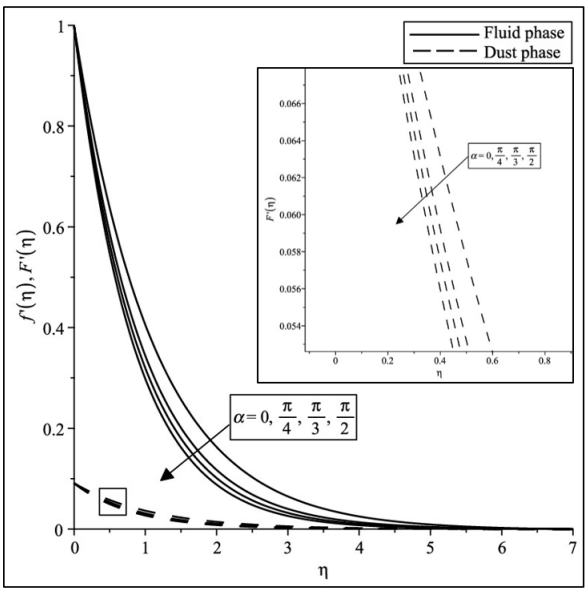


Figure 6: Velocity profiles for various values of $\alpha$.

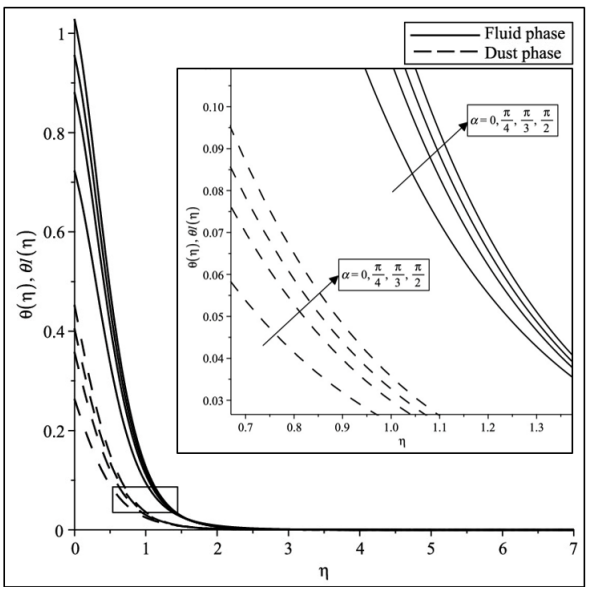


Figure 7: Temperature profiles for various values of $\alpha$.

Figures 8 and 9 provide the graphical results for the velocity and temperature profiles for several values of $\phi$ . A noticeable trend emerges from both figures, demonstrating that as the value of $\phi$ increases, the corresponding velocity and temperature profiles are increased. The rise of $\phi$ in both fluid and dust phases implies a higher density of fluid and dust particles which will enhance the momentum transfer and fluid motion. Moreover, the greater number of particles will produce more collisions and interactions which will enhance the heat transfer process as the thermal boundary layer thickness experiences an increasing trend. As a result, the fluid motion increases and the temperature rises along the profiles.

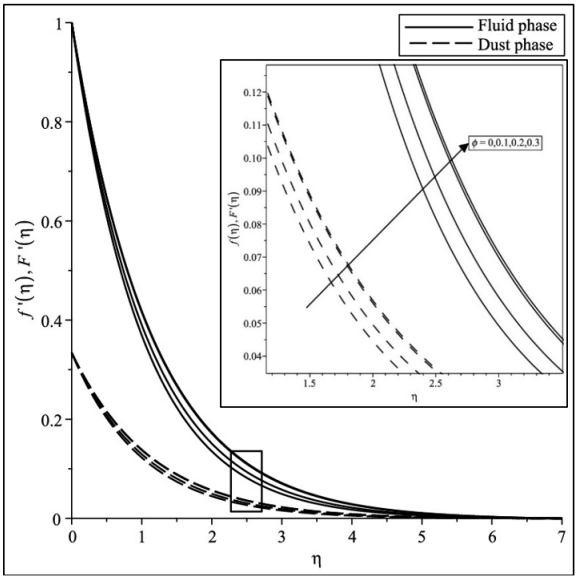


Figure 8: Velocity profiles for various values of $\phi$.

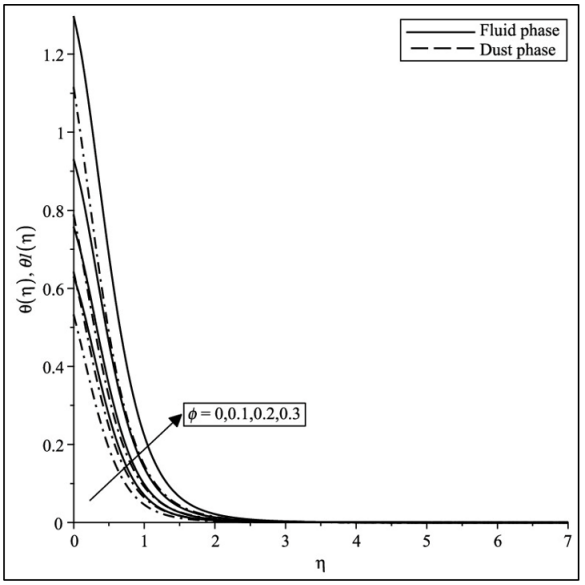


Figure 9: Temperature profiles for various values of $\phi$.

The influence of $\gamma$ on the velocity and temperature profiles for fluid and dust phases is illustrated in Figures 10 and 11. An insignificant change is observable in the velocity profiles, which can be attributed to the decoupling of the momentum and energy equations in both fluids. In contrast, the temperature profile shows improvement with a rise in $\gamma$ in both phases. From a physical standpoint, elevating the $\gamma$ enhances the efficiency of heat transfer coefficient which allows more effective thermal energy exchange between phases. This results in an increase in the thermal interaction which leads to an overall increase in temperature in both the fluid and dust phases.

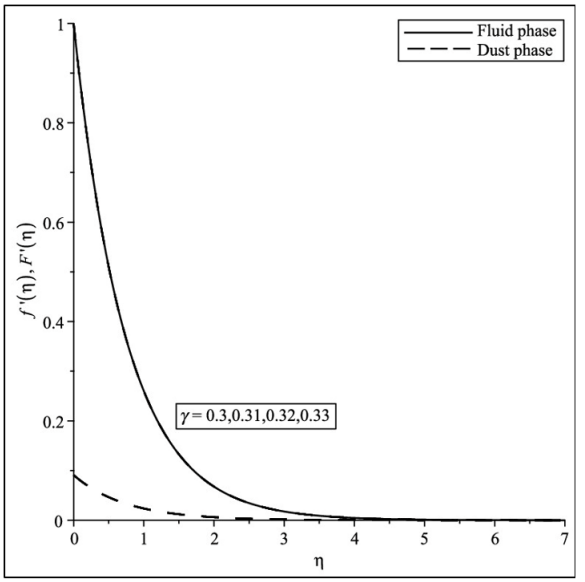


Figure 10: Velocity profiles for various values of $\gamma$.

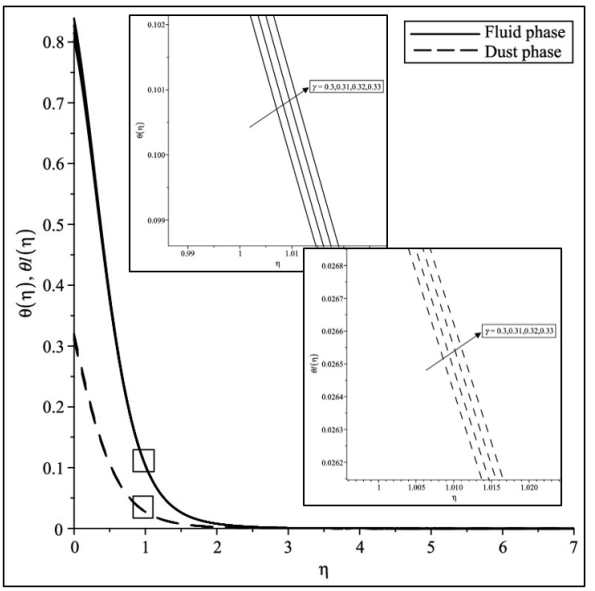


Figure 11: Temperature profiles for various values of $\gamma$.

Meanwhile, Figures 12 and 13 indicate the graph for the velocity and temperature profiles for different values of $\beta$. Figure 12 reveals that as $\beta$ increases, the velocity decreases for the fluid phase, while the opposite trend is observed in the dust phase. A similar trend can be spotted in the temperature profile for both phases, as shown in Figure 13 where it can be viewed that the temperature increases as value of $\beta$ rises. The reason for this behavior is that the fluid flows more slowly over the sheet as $\beta$ increases. This occurs because the relaxation time of dust particles also increases, causing the dust particles to move more rapidly, almost matching the fluid velocity. As a result, the dust particles create a drag (Stoke's Law) on the fluid when they come into contact and cause the fluid to decelerate.

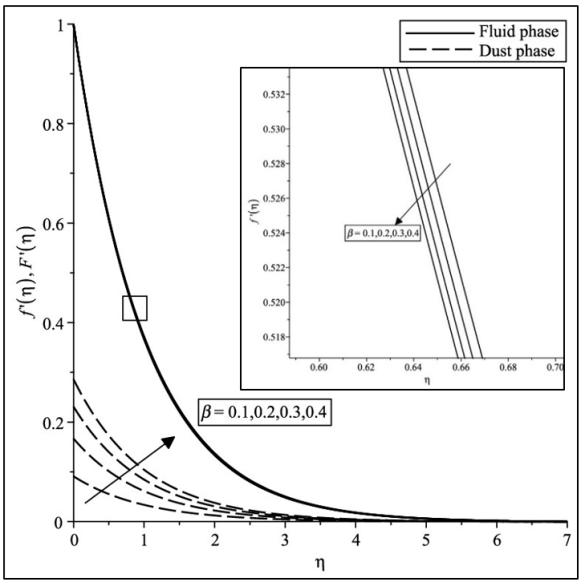


Figure 12: Velocity profiles for various values of $\beta$.

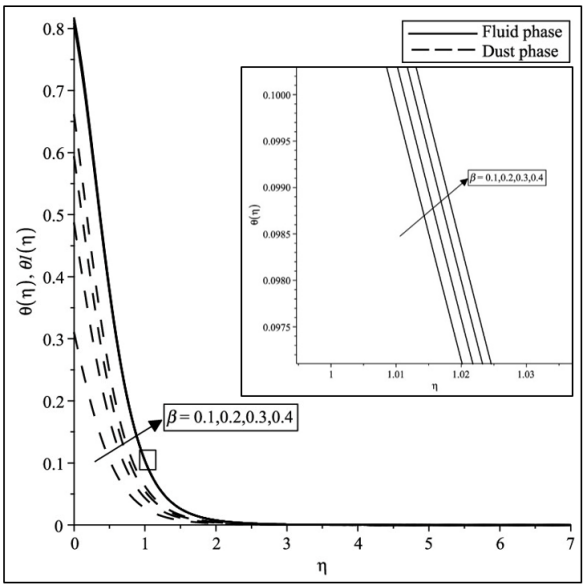


Figure 13: Temperature profiles for various values of $\beta$.

## 5 Conclusions

In this study, the emphasis lies on the critical role of fluid type in understanding its behaviour and interaction with surfaces. Considering this, the current study will focus on the non-Newtonian fluid that does not obey Newton's law of viscosity where the viscosity is not constant and depends on the shear rate. The mathematical formulation is predicated on the steady, incompressible and two-dimensional laminar flow of aligned MHD dusty Jeffrey fluid containing CNTs over an in-

clined stretching sheet with NH as the boundary condition. The investigation indicates that,

- An increase in the relevant parameters such as the $\alpha$, $\lambda$, $M$ and $\beta$ results in a depletion in the velocity profile of the fluid phase.
- A rise in $\phi$ and $\beta$ parameters of the dust phase result in an increase in velocity.
- The temperature profile displays a consistent rise for both the fluid and dust phases across all considered parameters, except for the $\lambda$ in fluid phase.
- The value of $-C_f Re_x{}^{\frac{1}{2}}$ increase as parameters $\beta$, $\phi$ and $De$ increases.
- As parameter $\lambda$ and $\gamma$ increases, the value of $Nu_x Re_x{}^{\frac{-1}{2}} X^{-1}$ shows an increment.

The analysis on the velocity and temperature profiles for both fluid and dust phases highlights the distinct behaviours within the system where the observed trends provide understanding on how these phases interact and respond to various parameters. For future work, it is recommended to explore the impact of additional factors on the studied system such as varying magnetic field strengths or different types of nanoparticles. Additionally, considering the three-dimensional effects could provide a more comprehensive understanding of the fluid dynamics.

**Acknowledgement** The authors gratefully acknowledge the financial support received in the form of fundamental research grants (FRGS) fund from the Ministry of Higher Educational, Malaysia, FRGS/1/2021/STG06/UITM/02/2.

**Conflicts of Interest** The authors declare no conflict of interest.

## References

[1] K. Ahmad & A. Ishak (2016). MHD flow and heat transfer of a Jeffrey fluid over a stretching sheet with viscous dissipation. *Malaysian Journal of Mathematical Sciences*, *10*(S), 311–323. https://mjms.upm.edu.my/lihatmakalah.php?kod=2016/February/10(S)//311-323.

[2] K. Ahmad & A. Ishak (2017). Magnetohydrodynamic (MHD) Jeffrey fluid over a stretching vertical surface in a porous medium. *Propulsion and Power Research*, *6*(4), 269–276. https://doi.org/10.1016/j.jppr.2017.11.007.

[3] J. Ahmed, A. Shahzad, M. Khan & R. Ali (2015). A note on convective heat transfer of an MHD Jeffrey fluid over a stretching sheet. *AIP Advances*, *5*(11), Article ID: 117117. https://doi.org/10.1063/1.4935571.

[4] N. S. Anuar, N. Bachok, N. M. Arifin & H. Rosali (2020). MHD flow past a nonlinear stretching/shrinking sheet in carbon nanotubes: Stability analysis. *Chinese Journal of Physics*, *65*, 436–446. https://doi.org/10.1016/j.cjph.2020.03.003.

[5] N. S. Anuar, N. Bachok & I. Pop (2018). A stability analysis of solutions in boundary layer flow and heat transfer of carbon nanotubes over a moving plate with slip effect. *Energies*, *11*(12), Article ID: 3243. https://doi.org/10.3390/en11123243.

[6] N. S. Anuar, N. Bachok, M. Turkyilmazoglu, N. M. Arifin & H. Rosali (2020). Analytical and stability analysis of MHD flow past a nonlinearly deforming vertical surface in Carbon Nanotubes. *Alexandria Engineering Journal*, *59*(1), 497–507. https://doi.org/10.1016/j.aej.2020.01.024.

[7] T. Anusha, U. S. Mahabaleshwar & S. Bhattacharyya (2023). An impact of MHD and radiation on flow of Jeffrey fluid with carbon nanotubes over a stretching/shrinking sheet with Navier's slip. *Journal of Thermal Analysis and Calorimetry*, *148*(22), 12597–12607. https://doi.org/10.1007/s10973-023-12588-1.

[8] H. A. Attia & K. M. Ewis (2019). Magnetohydrodynamic flow of continuous dusty particles and non-Newtonian Darcy fluids between parallel plates. *Advances in Mechanical Engineering*, *11*(6), 1687814019857349. https://doi.org/10.1177/1687814019857349.

[9] S. U. S. Choi & J. A. Eastman. Enhancing thermal conductivity of fluids with nanoparticles. Technical report Argonne National Laboratory, Argonne, IL United States 10 1995. https://www.osti.gov/biblio/196525.

[10] N. Dalir (2014). Numerical study of entropy generation for forced convection flow and heat transfer of a Jeffrey fluid over a stretching sheet. *Alexandria Engineering Journal*, *53*(4), 769–778. https://doi.org/10.1016/j.aej.2014.08.005.

[11] R. Devi, V. Poply & Manimala (2021). Effect of aligned magnetic field and inclined outer velocity in Casson fluid flow over a stretching sheet with heat source. *Journal of Thermal Engineering*, *7*(4), 823–844. https://dx.doi.org/10.18186/thermal.930347.

[12] M. Farooq, N. Gull, A. Alsaedi & T. Hayat (2015). MHD flow of a Jeffrey fluid with Newtonian heating. *Journal of Mechanics*, *31*(3), 319–329. https://doi.org/10.1017/jmech.2014.93.

[13] N. A. N. N. Habib, N. S. Arifin, S. M. Zokri & A. R. M. Kasim (2023). Aligned MHD Jeffrey fluid flow containing carbon nanoparticles over exponential stretching sheet with viscous dissipation and newtonian heating effects. *Journal of Advanced Research in Fluid Mechanics and Thermal Sciences*, *106*(1), 104–115. https://doi.org/10.37934/arfmts.106.1.104115.

[14] T. Hayat, S. Asad, M. Mustafa & A. Alsaedi (2015). MHD stagnation-point flow of Jeffrey fluid over a convectively heated stretching sheet. *Computers & Fluids*, *108*, 179–185. https://doi.org/10.1016/j.compfluid.2014.11.016.

[15] T. Hayat, G. Bashir, M. Waqas & A. Alsaedi (2016). MHD flow of Jeffrey liquid due to a nonlinear radially stretched sheet in presence of Newtonian heating. *Results in Physics*, *6*, 817–823. https://doi.org/10.1016/j.rinp.2016.10.001.

[16] T. Hayat, Z. Iqbal, M. Mustafa & A. Alsaedi (2014). Unsteady flow and heat transfer of Jeffrey fluid over a stretching sheet. *Thermal Science*, *18*(4), 1069–1078.

[17] A. Hussanan, M. Z. Salleh, H. T. Alkasasbeh & I. Khan (2018). MHD flow and heat transfer in a Casson fluid over a nonlinearly stretching sheet with newtonian heating. *Heat Transfer Research*, *49*(12), 1185–1198. https://doi.org/10.1615/HeatTransRes.2018014771.

[18] S. S. Ishak, N. N. M. N. Azhar, N. S. Nazli, M. R. Ilias, R. Osman, Z. Sadikin, A. R. M. Kasim & N. F. Mohammad (2023). Carbon nanotubes flow on mixed convection of aligned magnetohydrodynamics over a static/moving wedge with convective boundary conditions. *CFD Letters*, *15*(7), 74–91. https://doi.org/10.37934/cfdl.15.7.7491.

[19] S. N. H. Izani & A. Ali (2016). Mixed convective boundary layer flow of a dusty Jeffrey fluid over an exponentially stretching sheet. In *AIP Conference Proceedings*, volume 1775. AIP Publishing. https://doi.org/10.1063/1.4965177.

[20] S. N. H. Izani & A. Ali (2019). Thermal radiation effects on heat and mass transfer of magnetohydrodynamics dusty Jeffrey fluid past an exponentially stretching sheet. *Matematika*, *35*(2), 187–200. https://doi.org/10.11113/matematika.v35.n2.1172.

[21] A. R. M. Kasim, N. S. Arifin, S. M. Zokri & M. Z. Salleh (2019). Fluid-particle interaction with buoyancy forces on Jeffrey fluid with Newtonian heating. *CFD Letters*, *11*(1), 1–16. https://akademiabaru.com/submit/index.php/cfdl/article/view/3106.

[22] A. R. M. Kasim, N. S. Arifin, S. M. Zokri & M. Z. Salleh (2020). The investigation of a fluid-solid interaction mathematical model under combined convective jeffrey flow and radiation effect embedded newtonian heating as the thermal boundary condition over a vertical stretching sheet. In *Defect and Diffusion Forum*, volume 399 pp. 65–75. Trans Tech Publ. https://doi.org/10.4028/www.scientific.net/DDF.399.65.

[23] I. Khan (2019). New idea of Atangana and Baleanu fractional derivatives to human blood flow in nanofluids. *Chaos*, *29*(1), Article ID: 013121. https://doi.org/10.1063/1.5078738.

[24] I. Khan (2023). Ramped heating in CNTS fractional nanofluids. *Case Studies in Thermal Engineering*, *45*, Article ID: 102836. https://doi.org/10.1016/j.csite.2023.102836.

[25] I. Khan, A. M. Alqahtani, A. Khan, D. Khan, A. H. Ganie & G. Ali (2022). New results of fractal fractional model of drilling nanoliquids with clay nanoparticles. *Fractals*, *30*(1), Article ID: 2250024. https://doi.org/10.1142/S0218348X22500244.

[26] W. Khan, Z. Khan & M. Rahi (2014). Fluid flow and heat transfer of carbon nanotubes along a flat plate with Navier slip boundary. *Applied Nanoscience*, *4*, 633–641. https://doi.org/10.1007/s13204-013-0242-9.

[27] M. Kumar (2020). Study of differential transform technique for transient hydromagnetic Jeffrey fluid flow from a stretching sheet. *Nonlinear Engineering*, *9*(1), 145–155. https://doi.org/10.1515/nleng-2020-0004.

[28] O. D. Makinde (2010). Similarity solution of hydromagnetic heat and mass transfer over a vertical plate with a convective surface boundary condition. *International Journal of the Physical Sciences*, *5*(6), 700–710. https://doi.org/10.5897/IJPS.9000496.

[29] S. Manjunatha & B. J. Gireesha (2016). Effects of variable viscosity and thermal conductivity on MHD flow and heat transfer of a dusty fluid. *Ain Shams Engineering Journal*, *7*(1), 505–515. https://doi.org/10.1016/j.asej.2015.01.006.

[30] J. H. Merkin (1994). Natural-convection boundary-layer flow on a vertical surface with Newtonian heating. *International Journal of Heat and Fluid Flow*, *15*(5), 392–398. https://doi.org/10.1016/0142-727X(94)90053-1.

[31] A. R. Mohd Kasim, N. S. Arifin, S. Mohd Zokri, M. Z. Salleh, N. F. Mohammad, D. L. Chuan Ching, S. Shafie & N. A. N. Ariffin (2020). Convective transport of fluid–solid interaction: A study between non-Newtonian Casson model with dust particles. *Crystals*, *10*(9), Article ID: 814. https://doi.org/10.3390/cryst10090814.

[32] H. A. Nabwey, M. Mushtaq, M. Nadeem, M. Ashraf, A. M. Rashad, S. I. Alshber & M. A. Hawsah (2022). Note on the numerical solutions of unsteady flow and heat transfer of Jeffrey fluid past stretching sheet with Soret and Dufour effects. *Mathematics*, *10*(24), Article ID: 4634. https://doi.org/10.3390/math10244634.

[33] W. H. Press (2007). *Numerical Recipes*. The art of scientific computing. Cambridge University Press, Cambridge 3rd edition.

[34] G. B. Reddy, D. C. Kesavaiah, G. B. Reddy & N. Venu (2022). A note on heat transfer of MHD Jeffrey fluid over a stretching vertical surface through porous plate. *NeuroQuantology*, *20*(15), 3472–3486. https://www.neuroquantology.com/media/article_pdfs/3472-3486.pdf.

[35] D. A. Redwan, K. Karim, M. Mamun, M. K. A. Mohamed & S. M. Zokri. Boundary layer flow over a moving flat plate in Jeffrey fluid with Newtonian heating 2020. https://doi.org/10.48550/arXiv.2012.14417.

[36] K. U. Rehman, W. Shatanawi, S. Ashraf & N. Kousar (2022). Numerical analysis of Newtonian heating convective flow by way of two different surfaces. *Applied Sciences*, *12*(5), Article ID: 2383. https://doi.org/10.3390/app12052383.

[37] F. Shahzad, W. Jamshed, M. R. Eid, R. W. Ibrahim, F. Aslam, S. S. P. M. Isa & K. Guedri (2023). The effect of pressure gradient on MHD flow of a tri-hybrid Newtonian nanofluid in a circular channel. *Journal of Magnetism and Magnetic Materials*, *568*, Article ID: 170320. https://doi.org/10.1016/j.jmmm.2022.170320.

[38] R. K. Tiwari & M. K. Das (2007). Heat transfer augmentation in a two-sided lid-driven differentially heated square cavity utilizing nanofluids. *International Journal of Heat and Mass Transfer*, *50*(9–10), 2002–2018. https://doi.org/10.1016/j.ijheatmasstransfer.2006.09.034.

[39] I. Tlili (2019). Effects MHD and heat generation on mixed convection flow of Jeffrey fluid in microgravity environment over an inclined stretching sheet. *Symmetry*, *11*(3), Article ID: 438. https://doi.org/10.3390/sym11030438.

[40] D. A. Vallado (2001). *Fundamentals of Astrodynamics and Applications* volume 12. Springer Science & Business Media, United State.

[41] N. A. Zainal, R. Nazar, K. Naganthran & I. Pop (2021). MHD flow and heat transfer of hybrid nanofluid over a permeable moving surface in the presence of thermal radiation. *International Journal of Numerical Methods for Heat & Fluid Flow*, *31*(3), 858–879. https://doi.org/10.1108/HFF-03-2020-0126.

# Appendix A
## Derivation of Governing Equation for Fluid Phase

### A.1: Continuity Equation

The continuity equation can be written in vector notation which can be declared as the differential equation for the conservation law,

$$\frac{\partial \rho}{\partial t} + \bigtriangledown \cdot \rho V = 0.$$

For steady, viscous, incompressible, and two-dimensional fluid flow, $V = (u, v, 0)$, the equation becomes,

$$\frac{\partial u}{\partial x} + \frac{\partial v}{\partial y} V = 0.$$

### A.2: Momentum Equation

The momentum equation for fluid flow can be expressed in its conservative form as,

$$\rho\left(\frac{\partial V}{\partial t} + (V \cdot \bigtriangledown)V\right) = divT + \rho F_b.$$

The equation becomes,

$$\rho\left(u\frac{\partial u}{\partial x} + v\frac{\partial u}{\partial y}\right) = -\frac{\partial p_d}{\partial x} + \mu\left(\frac{\partial^2 u}{\partial x^2} + \frac{\partial^2 u}{\partial y^2}\right) - \sigma B_0^2 \sin^2 \alpha_1 u + (\rho_\infty - \rho)g.$$

The equation above is clearly appertaining and density differences $(\rho_\infty - \rho)$ is approximated into the following equation as,

$$(\rho_\infty - \rho) = \rho\beta^*(T - T_\infty).$$

Therefore, the momentum equation can be written as,

$$\left(u\frac{\partial u}{\partial x} + v\frac{\partial u}{\partial y}\right) = -\frac{1}{\rho}\frac{\partial p}{\partial x} + \frac{\mu}{\rho}\left(\frac{\partial^2 u}{\partial x^2} + \frac{\partial^2 u}{\partial y^2}\right) - \frac{\sigma}{\rho} B_0^2 \sin^2 \alpha_1 u + \beta^*(T - T_\infty)g.$$

### A.3: Energy Equation

The energy equation can be expressed as,

$$\rho c_p \frac{DT}{Dt} = k\left(\frac{\partial}{\partial x}\left(\frac{\partial T}{\partial x}\right) + \frac{\partial}{\partial y}\left(\frac{\partial T}{\partial y}\right) + \frac{\partial}{\partial z}\left(\frac{\partial T}{\partial z}\right)\right).$$

Alternatively, the above equation can be rewritten as,

$$\rho c_p\left(\frac{\partial T}{\partial t} + u\frac{\partial T}{\partial x} + v\frac{\partial T}{\partial y} + w\frac{\partial T}{\partial z}\right) = k\left(\frac{\partial^2 T}{\partial x^2} + \frac{\partial^2 T}{\partial y^2} + \frac{\partial^2 T}{\partial z^2}\right).$$

For steady 2D flow of incompressible fluid, energy equation can be written as,

$$\rho c_p\left(u\frac{\partial T}{\partial x} + v\frac{\partial T}{\partial y}\right) = k\left(\frac{\partial^2 T}{\partial x^2} + \frac{\partial^2 T}{\partial y^2}\right).$$

# Appendix B
## Derivation of Governing Equation for Dust Phase

The governing equations for dust phase consist of Continuity, Momentum and Energy Equations which can be expressed as;

$$\begin{aligned} \bigtriangledown \cdot V_p &= 0, \\ \rho_p(\frac{\partial V_p}{\partial t}) + V_p \cdot \bigtriangledown V_p &= -F_p, \\ \rho_p c_s (V \cdot \bigtriangledown) T_p &= -Q_p, \end{aligned}$$

where vector $V_p = (u_p, v_p, w_p)$ is the velocity field of dust particles. Substituting $F_p = \frac{\rho_p}{\tau_v}(V_p - V)$ and $Q_p = \frac{\rho_p C_s}{\tau_T}(T_p - T)$ to the above equation results in momentum and energy equation below. Therefore, the governing equation of dust phase can be written as;

$$\begin{aligned} \frac{\partial u_p}{\partial x} + \frac{\partial v_p}{\partial y} &= 0, \\ u_p \frac{\partial u_p}{\partial x} + v_p \frac{\partial v_p}{\partial y} &= -\frac{1}{\tau_v}(u_p - u), \\ u_p \frac{\partial T_p}{\partial x} + v_p \frac{\partial T_p}{\partial y} &= -\frac{1}{\tau_T}(T_p - T). \end{aligned}$$

# Appendix C
## Maple Sheet for RKF45 Method

```
> restart;
> with(plots):
> blt := 7:
> gam := 0.3:
> ϕ := 0.1:
> Pr := 7:
> M := 3:
> Ec := 0.3:
> #λ:=0.1:
> De := 0.2:
> α := π/6:
> αl := π/6:
> β := 0.5:
> N := 0.2:
> ρ_CNT := 2600:
> ρ_f := 1053:
> Cp_CNT := 425:
> Cp_f := 3594:
> k_CNT := 6600:
> k_f := 0.492:
> σ_CNT := (10)^6 - (10)^7:
> σ_f := 0.18:
> C_1 := 1/((1-ϕ) + ϕ·ρ_CNT/ρ_f):
> C_2 := 1 + 3·(σ_CNT/σ_f - 1)·ϕ / ((σ_CNT/σ_f + 2) - 3·(σ_CNT/σ_f - 1)·ϕ):
>
> C_3 := ((1-ϕ) + 2·ϕ·k_CNT/(k_CNT - k_f)·ln((k_CNT - k_f)/(2 k_f))) / ((1-ϕ) + 2·ϕ·k_CNT/(k_CNT - k_f)·ln((k_CNT + k_f)/(2 k_f))):
> C_4 := (1-ϕ) + ϕ·(ρ_CNT·Cp_CNT)/(ρ_f Cp_f):
> Eq1 := C_1·1/(1-ϕ)^2.5·(diff(f(η), η, η, η) + De·(-f(η)·diff(f(η), η, η, η) + (diff(f(η),
      η, η))^2)) + (1 + λ)·(-(diff(f(η), η))^2 + f(η)·diff(f(η), η, η)) - C_2/C_1·(1 + λ)·M
      ·diff(f(η), η)·(sin(α))^2 + (1 + λ)·d·θ(η)·cos(αl) + (1 + λ)·β·N·(diff(F(η), η)
      - diff(f(η), η)) = 0:
> Eq2 := 1/Pr·C_3/C_4·diff(θ(η), η, η) + f(η)·diff(θ(η), η) + 1/(1-ϕ)^2.5/(C_4·(1 + λ))·Ec·((diff(f(η), η,
```

```
      η))^2 + De·(diff(f(η), η)·(diff(f(η), η, η))^2 − f(η)·diff(f(η), η, η)·diff(f(η), η, η,
      η))) + β·N·c·(θl(η) − θ(η)) = 0:
> Eq3 := (diff(F(η), η))^2 − F(η)·(diff(F(η), η, η)) + β·(diff(F(η), η) − diff(f(η), η))
      = 0:
> Eq4 := (diff(θl(η), η))·F(η) − 2/3·β/(Pr·b)·(θl(η) − θ(η)) = 0:
>
> for k from 1 to 4 do R := dsolve(eval({Eq1, Eq2, Eq3, Eq4, bcs1}, λ = L[k]), [f(η), θ(η), F(η),
      θl(η)]): Y||k := rhs(R[2]): YA||k := rhs(R[3]): YB||k := rhs(R[4]): YC||k := rhs(R[5]): YD
      ||k := rhs(R[6]): YE||k := rhs(R[7]): YF||k := rhs(R[8]): YG||k := rhs(R[9]): YH||k :=
      rhs(R[10]):end do:
```